

Phase diagram of two-dimensional colloids with Yukawa repulsion and dipolar attraction

Cite as: J. Chem. Phys. **150**, 104903 (2019); <https://doi.org/10.1063/1.5082785>

Submitted: 24 November 2018 . Accepted: 15 February 2019 . Published Online: 08 March 2019

Nikita P. Kryuchkov , Frank Smallenburg , Alexei V. Ivlev , Stanislav O. Yurchenko , and Hartmut Löwen 



View Online



Export Citation



CrossMark

ARTICLES YOU MAY BE INTERESTED IN

Theory of coherent two-dimensional vibrational spectroscopy

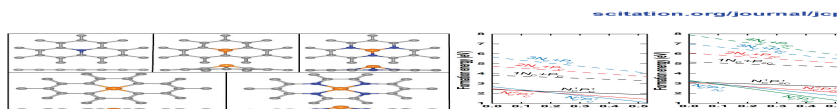
The Journal of Chemical Physics **150**, 100901 (2019); <https://doi.org/10.1063/1.5083966>

Perspective: Excess-entropy scaling

The Journal of Chemical Physics **149**, 210901 (2018); <https://doi.org/10.1063/1.5055064>

Common microscopic structural origin for water's thermodynamic and dynamic anomalies

The Journal of Chemical Physics **149**, 224502 (2018); <https://doi.org/10.1063/1.5055908>



Volume 150, Issue 10, 14 Mar 2019
Bifunctional mechanism of N, P co-doped graphene for catalyzing oxygen reduction and evolution reactions
 J. Chem. Phys. **150**, 104701 (2019); doi.org/10.1063/1.5082995
 Xiang-Xiong Xue, Li-Ming Tang, Keqiu Chen, Lixin Zhang, En-gu Wang, and Yexin Feng



Phase diagram of two-dimensional colloids with Yukawa repulsion and dipolar attraction

Cite as: J. Chem. Phys. 150, 104903 (2019); doi: 10.1063/1.5082785

Submitted: 24 November 2018 • Accepted: 15 February 2019 •

Published Online: 8 March 2019



View Online



Export Citation



CrossMark

Nikita P. Kryuchkov,¹  Frank Smallenburg,^{2,3}  Alexei V. Ivlev,⁴  Stanislav O. Yurchenko,^{1,a)} 
and Hartmut Löwen^{2,b)} 

AFFILIATIONS

¹Bauman Moscow State Technical University, 2nd Baumanskaya Street 5, 105005 Moscow, Russia

²Institut für Theoretische Physik II: Soft Matter, Heinrich-Heine-Universität Düsseldorf, Universitätsstrasse 1, 40225 Düsseldorf, Germany

³Laboratoire de Physique des Solides, CNRS, University of Paris-Sud, University of Paris-Saclay, 91405 Orsay, France

⁴Max-Planck-Institut für Extraterrestrische Physik, Giessenbachstrasse 1, 85748 Garching, Germany

^{a)}Electronic mail: st.yurchenko@mail.ru

^{b)}Electronic mail: hlowen@thphy.uni-duesseldorf.de

ABSTRACT

We study the phase diagram of a two-dimensional (2D) system of colloidal particles, interacting via an isotropic potential with a short-ranged Yukawa repulsion and a long-ranged dipolar attraction. Such interactions in 2D colloidal suspensions can be induced by rapidly rotating in-plane magnetic (or electric) fields. Using computer simulations and liquid integral equation theory, we calculate the bulk phase diagram, which contains gas, crystalline, liquid, and supercritical fluid phases. The densities at the critical and triple points in the phase diagram are governed by the softness of Yukawa repulsion and can therefore be largely tuned. We observe that the liquid-gas binodals exhibit universal behavior when the effective temperature (given by the inverse magnitude of the dipolar attractions) is normalized by its value at the critical point and the density is normalized by the squared Barker-Henderson diameter. The results can be verified in particle-resolved experiments with colloidal suspensions.

Published under license by AIP Publishing. <https://doi.org/10.1063/1.5082785>

I. INTRODUCTION

Colloidal suspensions in electric and magnetic fields open up spectacular opportunities for a wide range of fundamental and applied studies.¹⁻³ Two-dimensional (2D) colloidal crystals self-assembled in external fields can act as seeds for 3D structures used in photonics⁴⁻⁸ as well as for porous media and membranes used for photocatalysis, electrochemical energy storage and conversion, and chemical applications.⁹⁻¹³ Although tunable interactions can be achieved in different ways (including optical, chemical, and flow-mediated mechanisms²), the use of electric¹⁴⁻²⁹ and magnetic^{16,30-41} fields is among the most promising due to their technological flexibility, the long-range character of the obtained interactions, and the ability to change them *in situ*.

From a fundamental point of view, colloidal suspensions with tunable interactions allow us to perform particle-resolved studies^{1,2,42-45} to understand basic generic mechanisms of melting and crystallization, condensation and evaporation, spinodal decomposition, slow dynamics in glasses, nucleation, and coalescence, occurring in different regimes of interactions between particles.^{1,26,43,46-48}

Dipolar attractions induced by external rotating fields have attracted interest in the framework of particle-resolved studies of 2D systems in magnetic^{32,35,48} and electric^{18,25,26,49} fields. These studies used 2D colloidal suspensions of particles, which were synchronously polarized by an in-plane rotating field, yielding isotropic dipolar attractions $\propto 1/r^3$ at large distances, whose magnitude is determined by the field magnitude and the material properties of the solvent and colloids.⁵⁰ At short distances (near the contact

between the particles), the basic interaction (without the external fields) is described by Derjaguin, Landau, Verwey, and Overbeek (DLVO) theory.^{2,51} In charge-stabilized colloids, where the dominant interaction is the Yukawa (Debye-Hückel) repulsion, the phase states, collective dynamics, and thermodynamics have been studied in detail in Refs. 52–64. Experimentally, the Yukawa repulsion can be “adjusted” using charge regulation by varying the choice of solvent, salt concentration, and material properties of the colloidal surface.⁵¹

The addition of an attracting dipolar branch to the short-range repulsion between colloids diversifies the phase behavior of the system and leads to the emergence of a liquid-gas binodal and a corresponding critical point. Clustering and coarsening of such systems has been studied using computer simulations of a model 2D system of rotating permanent dipoles with fixed inverse power law repulsion^{65–67} and in 2D Stockmayer fluids.⁶⁸ Additionally, the 3D phase diagram of a model system with isotropic Yukawa repulsion and anisotropic inverse-dipolar interaction was studied in Ref. 69. However, we are not aware of papers reporting on the detailed calculation of phase diagrams of 2D systems with Yukawa repulsion and dipolar attraction between particles and, in particular, on the role of Yukawa repulsion softness, which is determined as ratio of the screening length to the particle diameter.

In this work, we explore the phase diagram of 2D colloidal systems of particles interacting via Yukawa repulsion at short distances and isotropic dipolar attraction at large distances. We show that the phase diagram of the system contains crystal, liquid, and gas phases and a supercritical fluid. The spinodal is calculated using Ornstein-Zernike theory, and the results for the critical point parameters agree well with those from binodal branches. We used Monte-Carlo (MC) and molecular dynamics (MD) simulations to analyze the near-critical behavior and to study the bulk phase diagram of the system for different characteristic magnitudes of repulsive and attractive parts of the interaction. We observed that the dimensionless densities and effective temperatures (determined by dipolar attraction) at the critical and triple points in the phase diagram depend significantly on the softness of the Yukawa repulsion. Moreover, we show that the phase diagrams at different repulsion softness can be mapped to the phase diagram of hard disks with isotropic dipolar attraction by normalizing the density and the effective temperature with the inverse squared Barker-Henderson diameter and the critical temperature. In this mapping, the liquid-gas binodals exhibit universal behavior, almost insensitive to the repulsion softness, while the form of crystalline binodals is changed significantly. Finally, we discuss the experimental realization of the studied system with tunable magnetic interactions.

II. SYSTEM AND METHODS

A. System

Consider a 2D suspension of monodisperse spherical colloidal particles in a surrounding medium (solvent). According to the DLVO theory, the electrostatic interaction between the particles is described by a Yukawa (screened Coulomb or Debye-Hückel) repulsion.² We assume that the colloidal suspension is stabilized by a fairly large charge of the particles, which inhibits the close approach

of the particles, so that we can neglect the short-range van der Waals attraction.

The externally applied in-plane rotating electric or magnetic field polarizes the particles and induces an additional (tunable) long-range dipolar attraction.^{32,50} We assume that the particle properties are independent of the magnitude of the field and that the tunable effective interactions can be considered in the dipolar approximation. Then, in fast-rotating fields, the anisotropic part of interactions vanishes after angular averaging and only the dipolar attraction remains. Here, the time period of the rotating field needs to be much shorter than the diffusive scale of colloid motion but much longer than the diffusion time of the microscopic counterions which establish the electrostatic screening. We remark that, to obtain equilibrium phase diagrams of the system, hydrodynamic interactions can be neglected.⁶⁶

In our model, the interactions in the system are described by the following pair potential:

$$\begin{aligned}\varphi(r) &= \varphi_Y(r) + \varphi_D(r), \\ \varphi_Y(r) &= \begin{cases} \infty, & r/\sigma < 1; \\ \varepsilon_Y \frac{\exp[-\kappa\sigma(r/\sigma - 1)]}{r/\sigma}, & r/\sigma > 1, \end{cases} \\ \varphi_D(r) &= -\varepsilon_D \left(\frac{\sigma}{r}\right)^3, \end{aligned} \quad (1)$$

where $\varphi_Y(r)$ and $\varphi_D(r)$ correspond to the hard core Yukawa repulsion and dipolar attraction with magnitudes ε_Y and $\varepsilon_D \propto H^2$ (here H is the magnitude of rotating magnetic field), respectively, σ is the particle diameter, and $\kappa = 1/\lambda$ is the inverse Debye screening length in the solvent. In the linear screening regime, the magnitude ε_Y of the Yukawa potential is related to the charge of colloid as

$$\beta\varepsilon_Y = \frac{Z^2}{(1 + \kappa\sigma/2)^2} \frac{\lambda_B}{\sigma}, \quad (2)$$

where $\beta = 1/k_B T$ is the inverse temperature in energy units, T is the temperature, k_B is Boltzmann's constant, Z is the number charge of the colloid, and $\lambda_B = e^2/4\pi\epsilon_0\epsilon_S k_B T$ is the Bjerrum length related to the Debye-Hückel inverse screening length $\kappa = \sqrt{4\pi\lambda_B n_i}$, where n_i is the total number density of (monovalent) ions in the solvent, e is the elementary charge, ϵ_0 is the vacuum dielectric constant, and ϵ_S is the relative dielectric constant of the solvent.

In the regime of strongly charged colloids, the linear Poisson-Boltzmann approach becomes unsuitable.⁷⁰ The nonlinear effects are confined to the vicinity of the particle surface in the layer of thickness λ , which is assumed to be much smaller than σ . In this case, the functional form of the repulsion remains the same, but with the effective (renormalized) charge Z_{eff} ⁷⁰

$$Z_{\text{eff}} = \frac{4\sigma}{\lambda_B} \frac{(1 + \kappa\sigma/2)^2}{1 + \kappa\sigma}, \quad (3)$$

which should be used in Eq. (2) instead of Z that yields

$$\beta\varepsilon_Y = \frac{16\sigma}{\lambda_B} \left(\frac{1 + \kappa\sigma/2}{1 + \kappa\sigma}\right)^2. \quad (4)$$

Similarly to Ref. 18, we used in the following MC and MD simulations the value $\sigma/\lambda_B = 1043$ that corresponds to ≈ 750 -nm-diameter

particles in an aqua-based solvent ($\lambda_B = 7.2 \text{ \AA}$). However, in case of non-polar solvents, the corresponding diameter σ can be much larger.

One can see in Eq. (1) that the Yukawa repulsion vanishes at $\kappa\sigma \rightarrow \infty$, thus, reducing the interaction to

$$\beta\varphi_{\text{HDD}}(r) = \begin{cases} \infty, & r/\sigma < 1; \\ -\beta\epsilon_D(\frac{\sigma}{r})^3, & r/\sigma > 1, \end{cases} \quad (5)$$

which corresponds to a system of hard disks with isotropic dipolar attractions. The phase diagram of this system can be presented in the dimensionless coordinates of $\tilde{T} = 1/\beta\epsilon_D$, playing the role of effective temperature, and $\rho\sigma^2$.⁷¹ Although in systems with finite values of $\kappa\sigma$ the (dimensionless) potential $\beta\varphi(r)$ depends on \tilde{T} , one can still use \tilde{T} as a state parameter, which modulates the strength of the dipolar attraction.

Figure 1 illustrates $\beta\varphi(r)$ corresponding to $\kappa\sigma = 5$ and 19 at different values of \tilde{T} . One can see that increasing $\kappa\sigma$ enhances the asymmetry of the potential well near its minimum. The tunable term $\beta\varphi_D(r)$ is determined by the magnitude of the rotating magnetic field and can be changed in a broad range, while the (true) temperature T of the system is determined by the solvent bath.

B. MC and MD simulations

To obtain the phase diagram of the system, we used MC simulations in combination with free-energy calculations.⁷² Specifically, we mapped out the phase diagram as a function of the number density ρ and the dipolar attraction magnitude $\beta\epsilon_D$ for different fixed forms of the Yukawa repulsion, as determined by $\kappa\sigma$. We make use of thermodynamic integration⁷² to obtain free energies of all competing phases (fluid, gas, liquid, and solid). In this approach, the

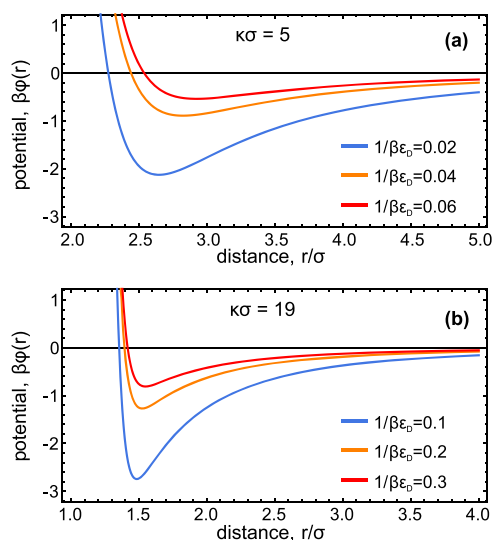


FIG. 1. Tunable pair potential. Panels (a) and (b) represent the characteristic form of the potential (1) used in simulations (at $\kappa\sigma = 5$ and $\kappa\sigma = 19$, respectively), plotted for different magnitudes of the effective temperature $\tilde{T} = 1/\beta\epsilon_D$.

free-energy difference between two state points is written as integrals over a path through parameter space of quantities that can be directly measured in our MC simulations, specifically the energy and pressure. All simulations are performed in the canonical (NVT) ensemble, i.e. at a constant number of particles N , volume V , and effective temperature T . We measure the pressure using the standard virial expression.⁷² Long-range interactions were truncated and shifted to zero at a fixed, sufficiently large cutoff range which was adapted to the screening length. All systems contained at least $N = 500$ particles.

For the gas, liquid, and fluid phases, we use the hard-disk fluid as a reference system. Specifically, the Helmholtz free energy of the hard-disk fluid at number density ρ is determined as

$$\frac{\beta F_{\text{HD}}(\rho)}{N} = \frac{\beta F_{\text{id}}(\rho)}{N} + \int_0^\rho d\rho' \frac{\beta P_{\text{HD}}(\rho') - \rho'}{\rho'^2}. \quad (6)$$

Here, N is the number of particles and $P_{\text{HD}}(\rho)$ is the hard-disk pressure at density ρ , for which we use an analytical approximation.⁷³ $F_{\text{id}}(\rho)$ is the ideal-gas free energy at density ρ , given by $\beta F_{\text{id}}(\rho) = N(\log(\rho\Lambda^3) - 1)$, with Λ the thermal wavelength, which does not affect the phase behavior. We then determine the free energy of a reference state of the charged system by considering the free-energy difference between the hard-disk system, where $\epsilon_Y = 0$, and the charged system (without external field), where ϵ_Y is given by Eq. (2). This free-energy difference is given by

$$F(\rho, \epsilon_D = 0) - F_{\text{HD}}(\rho) = \int_0^{\epsilon_Y} d\epsilon_Y' \langle U_Y/\epsilon_Y' \rangle, \quad (7)$$

where $\langle U_Y/\epsilon_Y' \rangle$ is the averaged total potential energy of a system (divided by ϵ_Y'), measured in a simulation where the prefactor for the Yukawa potential is set to ϵ_Y' . To obtain free energies $\beta F(\rho, \epsilon_D)$ in the gas, liquid, and fluid phases at different densities and dipolar interaction strengths, we again employ thermodynamic integration, using

$$F(\rho_2, \epsilon_D) - F(\rho_1, \epsilon_D) = N \int_{\rho_1}^{\rho_2} d\rho' \frac{P(\rho', \epsilon_D)}{\rho'^2}, \quad (8)$$

$$F(\rho, \epsilon_{D,1}) - F(\rho, \epsilon_{D,2}) = \int_{\epsilon_{D,1}}^{\epsilon_{D,2}} d\epsilon_D' \left\langle \frac{U_D(\rho, \epsilon_D')}{\epsilon_D'} \right\rangle. \quad (9)$$

Here, $P(\rho, \epsilon_D)$ and $\langle U_D(\rho, \epsilon_D) \rangle$ are the average pressure and total dipolar energy, respectively. Together, Eqs. (8) and (9) allow us to calculate free energies at any density and effective temperature as long as we do not cross phase boundaries along the integration path.

For the crystal phase, we use the Frenkel-Ladd method⁷⁴ to obtain a reference free energy. After obtaining the reference free energy, we again use Eqs. (8) and (9) to calculate the free energy throughout the crystal phase.

Finally, we construct phase boundaries using the common-tangent approach.⁷² For a fixed dipolar interaction strength ϵ_D , we plot the free energy per volume $F(\rho, \epsilon_D)/V$ as a function of the density ρ and find pairs of points connecting different phases such that the slope and the intercept of the tangent lines are equal at the two points. This is equivalent to finding points of equal pressure and chemical potential and hence corresponds to finding the two densities associated with a first-order phase transition at a given effective temperature. Repeating this process at different temperatures then yields a full phase diagram of the system.

As an extra check on our results for liquids-gas binodals at different $\kappa\sigma$, we performed MD simulations in the canonical (*NVT*) ensemble with $N = 21\,600$ particles in a rectangular box with the sizes $L_x \times L_z = (60 \times 360)\rho_0^{-1/2}$. We used periodic boundary conditions and a cutoff radius of $r_c = 15\rho_0^{-1/2}$, where $\rho_0 = (0.02 \dots 0.2)\sigma^{-2}$ is the initial number density of the system. Using the Langevin thermostat, the system was equilibrated for the first 5×10^5 steps of $\Delta t = 5 \times 10^{-3}\sqrt{m\beta\sigma^2}$ (here m is the particle mass), while the following 10^6 steps were used for the further analysis.

The liquid-gas binodals were calculated using the plane layer method, which is standard for MD simulations.^{26,72,75} After equilibration, the density of the layer (normal to the z -axis) was fitted by the following profile:

$$\rho(z) = \frac{\rho_l + \rho_g}{2} - \frac{\rho_l - \rho_g}{2} \tanh\left(\frac{2(z-l)}{d}\right), \quad (10)$$

where ρ_l and ρ_g are the densities of the liquid and the gas, while the parameters l and d characterize the thickness of the layer and interface between the phases, respectively.

The triple points were estimated by extrapolating the gas-liquid and liquid-crystal binodals to their crossing point. The critical points were obtained by fitting the liquid and gas binodal branches near the critical point as follows:

$$\begin{aligned} \rho_l - \rho_g &\approx A(\tilde{T}_{\text{CP}} - \tilde{T})^{\beta_c}, \\ \frac{\rho_l + \rho_g}{2} &\approx \rho_{\text{CP}} + a(\tilde{T}_{\text{CP}} - \tilde{T}), \end{aligned} \quad (11)$$

where \tilde{T}_{CP} and ρ_{CP} are the effective temperature and density at the critical point, respectively, β_c is the critical exponent, and A and a are free parameters. According to Ref. 76, the universality class of a system depends on the range of potential attraction and, in the case of the long-range attraction $\propto 1/r^3$, the system exhibits classical critical (mean-field) behavior with $\beta_c = 1/2$. Importantly, for the calculation of the critical point parameters using the fitting functions in Eq. (11), we consider only the parts of the binodal lines which are unaffected by finite-size effects.

C. Ornstein-Zernike theory for spinodal

We complemented our MC and MD results by calculations of spinodals based on the Ornstein-Zernike (OZ) theory. Assuming that pair correlations can be described by the OZ equation in vicinity of the critical point,⁷⁷

$$h(r) = c(r) + \rho \int d\mathbf{r}' h(|\mathbf{r} - \mathbf{r}'|)c(r'), \quad (12)$$

where $h(r) = g(r) - 1$ and $g(r)$ and $c(r)$ are radial and direct correlation functions, respectively. As a closure relation for Eq. (12), we used the Percus-Yevick approximation⁷⁷

$$\begin{aligned} c(r) &= (1 + \Gamma(r))(\exp(-\beta U(r)) - 1), \\ \Gamma(r) &= h(r) - c(r). \end{aligned} \quad (13)$$

To determine the spinodal line, we solve Eqs. (12) and (13) at different densities and magnitudes of dipolar attraction to find the points at which

$$\frac{\partial(\beta P)}{\partial \rho} = 0, \quad (14)$$

where the left-hand side can be calculated using the direct correlation function $c(r)$ as

$$\frac{\partial(\beta P)}{\partial \rho} = 1 - \rho \int d\mathbf{r} c(r). \quad (15)$$

III. RESULTS

Figure 2 represents phase diagrams of the 2D model system in wide range of densities and effective temperatures, shown at $\kappa\sigma = 2, 5, 15$, and 19 in panels (a)–(d), respectively. The orange circles in Fig. 2 are obtained by MC simulations, while MD results for liquid-gas binodals are shown by red rhombi and one can see excellent agreement between the MC and MD simulations. Blue down triangles are spinodals obtained by OZ theory, orange triangles correspond to the median density $(\rho_l + \rho_g)/2$, while the black solid lines are linear fits. Blue solid lines are fits for binodals, while the horizontal dashed red lines mark the effective temperatures of triple points (TPs), whose densities and effective temperatures are presented in Table I for different values of $\kappa\sigma$. The liquid-gas binodals in the vicinity of critical point were obtained using the fit by Eq. (11). Note that, in the cases of $\kappa\sigma = 15$ and 19 , MD and MC points calculated for systems of different sizes are close to each other, justifying that the finite-size effects are negligible.

Comparing the results for different $\kappa\sigma$ in Fig. 2, one can see that the general form of the phase diagrams is similar and includes domains of crystal, gas, liquid, and supercritical states as well as domains of phase coexistence. In terms of the normalized density $\rho\sigma^2$, the width of the liquid-crystal coexistence area grows significantly with an increase in $\kappa\sigma$ from 0.003 at $\kappa\sigma = 2$ to 0.03 at $\kappa\sigma = 19$. The liquid-gas decomposition is well-described by parabolic fits for the binodals in the vicinity of the critical points and agrees completely with classical (“mean-field”) critical behavior. The average densities $(\rho_l + \rho_g)/2$ exhibit linear dependencies for all $\kappa\sigma$. The spinodals obtained from OZ theory yield parameters of the critical point which are very close to those obtained from the fit of liquid-gas binodals except at high $\kappa\sigma$.

Comparing the data presented in Table I, one can see that the repulsion softness (determined by $1/\kappa\sigma$) strongly affects the effective temperatures and normalized densities at the critical and triple points. For instance, \tilde{T}_{CP} and $\rho_{\text{CP}}\sigma^2$ increase about 36 and 10 times, respectively, with an increase in $\kappa\sigma$ from 2 to 19. Similar trends are observed for the temperatures and densities of the triple points. Surprisingly, the ratios $\tilde{T}_{\text{CP}}/\tilde{T}_{\text{TP}}$ and $\rho_{\text{TP}}/\rho_{\text{CP}}$ between the effective temperatures and densities at critical and triple points do not depend much on $\kappa\sigma$, as one can see in Table I.

Figure 2 demonstrate that the results for the critical point given by MC, MD, and OZ-PY approaches agree with each other for soft Yukawa repulsion. Interestingly, the PY closure relation is usually applied for systems of hard spheres. Motivated by this fact, we found that the phase diagrams in Fig. 2 can be mapped onto the phase diagram of the hard disks with isotropic dipolar attraction that we calculated using MC simulations in the same manner as the diagrams in Fig. 2.

To normalize the densities, we calculated the Barker-Henderson diameter, defined as⁷⁷

$$\sigma_{\text{BH}} = \int_0^{r_{\text{min}}} (1 - f(r))dr, \quad (16)$$

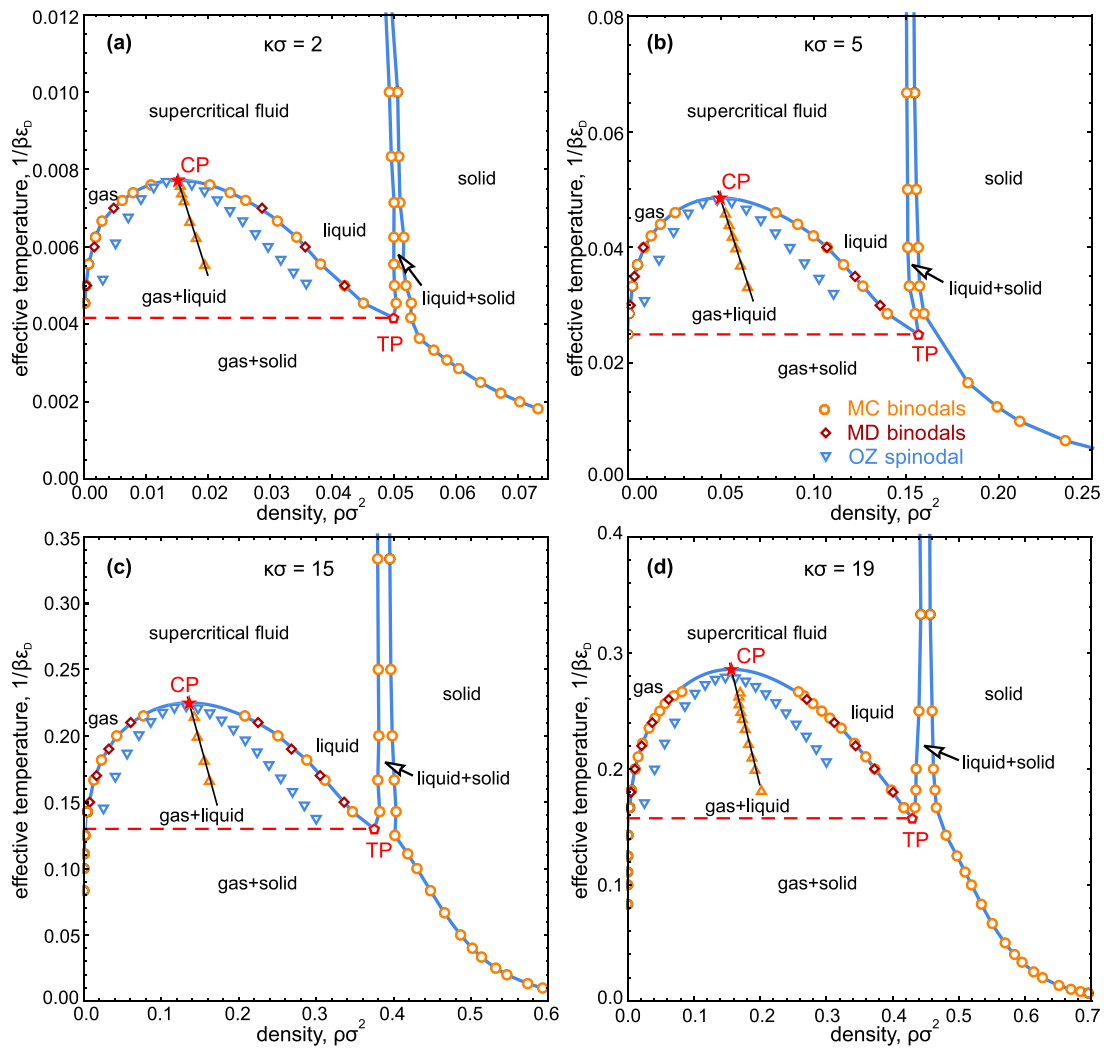


FIG. 2. Phase diagram at different $\kappa\sigma$ -values. Panels (a)–(d) represent the phase diagrams in the plane $(\rho\sigma^2, 1/\beta\epsilon_D)$ calculated at $\kappa\sigma = 2, 5, 15,$ and $19,$ respectively. Orange circles are binodals obtained by MC, red rhombi are MD results for liquid-gas binodals, and blue down triangles are obtained by OZ-PY theory for spinodal. Orange triangles correspond to the median density $(\rho_l + \rho_g)/2,$ while the solid black lines are linear fits. The solid blue lines are fits of binodals, and CP and TP indicate the effective critical and triple points, respectively.

where $f(r) = \exp[\beta\varphi(r_{\min}) - \beta\varphi(r)],$ and r_{\min} is the distance at which $\varphi(r)$ has a minimum. Note that $\sigma_{\text{BH}}(\kappa\sigma, \tilde{T})$ depends on the effective temperature $\tilde{T},$ but not on the density,

and $\sigma_{\text{BH}} \rightarrow \sigma$ at $\kappa\sigma \rightarrow \infty$ (the hard disk limit). The effective temperatures \tilde{T} were normalized to their critical values $\tilde{T}_{\text{CP}}(\kappa\sigma).$

TABLE I. Parameters of triple and critical points at different $\kappa\sigma.$

$\kappa\sigma$	\tilde{T}_{CP}	$\rho_{\text{CP}}\sigma^2$	\tilde{T}_{TP}	$\rho_{\text{TP}}\sigma^2$	$\tilde{T}_{\text{CP}}/\tilde{T}_{\text{TP}}$	$\rho_{\text{TP}}/\rho_{\text{CP}}$
1	1.54×10^{-3}	4.76×10^{-3}	7.414×10^{-4}	0.0188	2.08	3.95
2	7.72×10^{-3}	0.0152	4.16×10^{-3}	0.05	1.85	3.29
5	0.049	0.05	0.025	0.157	1.94	3.15
15	0.225	0.136	0.136	0.375	1.73	2.76
19	0.286	0.156	0.157	0.43	1.82	2.75

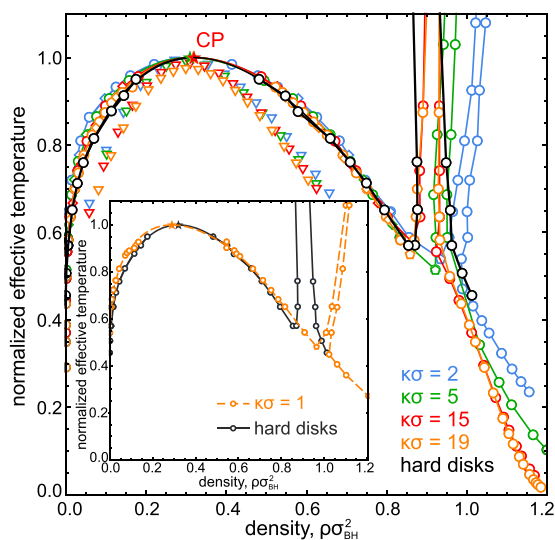


FIG. 3. Mapping to the phase diagram of hard disks with dipolar attraction. Black symbols and solid lines correspond to the phase diagram of hard disks with dipolar attraction, while the colored symbols and lines are normalized results from Fig. 2 for different $\kappa\sigma$ (see text for details of the normalization). The inset highlights a rapidly increasing deviation of the shown results from the hard-disk diagram at smaller $\kappa\sigma$.

Figure 3 represents our main result—the mapping of the phase diagrams, where the black symbols and lines represent the hard-disk model and the colored symbols and lines correspond to different $\kappa\sigma$. One can see that the liquid-gas binodals and spinodals show a remarkable universality at different softness of Yukawa repulsion with particularly good agreement for the liquid branch of the binodals.

The crystalline branches of the binodals are expected to depend strongly on the Yukawa repulsion softness since collective dynamics and thermodynamics at high densities are determined mainly by the repulsive branch. For instance, the detailed scenario of the melting in 2D systems depends on the repulsion softness and can include different phase transitions between crystalline, hexatic, and liquid phases.^{78–81} A detailed study of the freezing scenario is left for future studies.

Deviations from the hard-disk diagram in Fig. 3 grow monotonically with increasing softness of the Yukawa repulsion. To highlight this trend, in the inset, we present the MC phase diagrams for the two extreme cases considered in our simulations—hard disks (solid lines) and soft disks at $\kappa\sigma = 1$ (orange dashed lines). One can see that at smaller $\kappa\sigma$, the normalized density at the gaseous branch of the binodal slightly decreases, while the density of triple point and crystalline branch of binodal increase more significantly. Conversely, the liquid branch of the binodal is practically insensitive to the softness of Yukawa repulsion.

IV. CONCLUSIONS

To summarize, we calculated the phase diagram of a two-dimensional system with isotropic short-range Yukawa repulsion

and long-range dipolar attraction between particles. Using MC and MD simulations, as well as OZ theory with the PY closure relation, we computed the solid, fluid, gas, and supercritical equilibrium phases. Analysis of the diagrams indicates that the softness of Yukawa repulsion significantly affects the positions of the critical and triple points as well as the behavior of the crystalline branches of the binodals. At the same time, the liquid-gas binodals and spinodals can be mapped onto those for a system of hard disks with dipolar attraction, demonstrating a remarkable universality at different softnesses of the Yukawa repulsion.

The phase diagrams in Figs. 2 and 3 are plotted in the plane of the effective temperature, which is determined by the magnitude of the dipolar attraction, and the density. In contrast to typical systems, where the form of potential is fixed at different temperatures, the form of potential (1) changes at short distances with the increase in \tilde{T} , as illustrated in Fig. 1. However, the near-critical behavior is determined by the long-wavelength fluctuations of density,⁸² and, therefore, only long-range asymptotic of the potential is important. Since $\beta\varphi(r) \propto \tilde{T}^{-1}(\sigma/r)^3$ at large distances, \tilde{T} plays the same role as the kinetic temperature in systems with fixed interaction potential. We observe that the liquid-gas binodal is well described by a parabolic fit in the vicinity of the critical point, in accordance with classical (mean-field) critical behavior.

Our model can be realized in colloidal suspension exposed to rotating electric or magnetic fields. The tunable interactions in such systems have been thoroughly analyzed in Ref. 50, where it has been shown that three-body interactions become significant (up to ~60% comparing to the pair energy) at distances smaller than two particle diameters, while the many-body effects of higher orders can be neglected.^{32,35,50} Therefore, the relevant experimental conditions can be satisfied for 2D suspensions of particles having a magnetic core and nonmagnetic shell and exposed to rapidly rotating in-plane magnetic fields. The thickness of the nonmagnetic shell should not be (at least) about a half of the core diameter. In this case, the shell plays a role of a spacer between the interacting cores, thus inhibiting many-body effects. This can be achieved, for instance, by using suspensions of carboxyl-coated superparamagnetic polystyrene particles with the diameter of (2–3) μm and a magnetic core of about (1–1.5) μm in experiments following a protocol similar to that in Ref. 48. Phase states at different magnitudes of rotating magnetic fields and densities can be analyzed using, for example, the method for phase identification.²⁶ The derived phase diagram can then be directly compared with results of the present paper.

We believe that our paper will stimulate experimental and theoretical studies of tunable colloids in rotating fields and will be useful for understanding the role of interplay between short-range repulsion and long-range attraction in the phase behavior of 2D systems.

ACKNOWLEDGMENTS

MD calculations and analysis were supported by the Russian Science Foundation Grant No. 17-19-01691, and MC simulations were supported by the German Research Foundation (DFG) under Nos. LO 418/23-1 and IV 20/3-1.

REFERENCES

- ¹A. Ivlev, H. Löwen, G. Morfill, and C. P. Royall, *Complex Plasmas and Colloidal Dispersions: Particle-Resolved Studies of Classical Liquids and Solids*, Series in Soft Condensed Matter (World Scientific, Singapore, 2012).
- ²A. Fernandez-Nieves and A. M. Puertas, *Fluids, Colloids, and Soft Materials: An Introduction to Soft Matter Physics* (Wiley, 2016).
- ³J. Dobnikar, A. Snezhko, and A. Yethiraj, *Soft Matter* **9**, 3693 (2013).
- ⁴A. Yethiraj, J. Thijssen, A. Wouterse, and A. van Blaaderen, *Adv. Mater.* **16**, 596 (2004).
- ⁵X. Tang, B. Rupp, Y. Yang, T. D. Edwards, M. A. Grover, and M. A. Bevan, *ACS Nano* **10**, 6791 (2016).
- ⁶K. I. Zaytsev and S. O. Yurchenko, *Appl. Phys. Lett.* **105**, 051902 (2014).
- ⁷K. I. Zaytsev, G. M. Katyba, E. V. Yakovlev, V. S. Gorelik, and S. O. Yurchenko, *J. Appl. Phys.* **115**, 213505 (2014).
- ⁸S. O. Yurchenko, K. I. Zaytsev, E. A. Gorbunov, E. V. Yakovlev, A. K. Zotov, V. M. Masalov, G. A. Emelchenko, and V. S. Gorelik, *J. Phys. D: Appl. Phys.* **50**, 055105 (2017).
- ⁹A. Stein, B. E. Wilson, and S. G. Rudisill, *Chem. Soc. Rev.* **42**, 2763 (2013).
- ¹⁰M. Curti, J. Schneider, D. W. Bahnemann, and C. B. Mendive, *J. Phys. Chem. Lett.* **6**, 3903 (2015).
- ¹¹G. Collins, E. Armstrong, D. McNulty, S. O'Hanlon, H. Geaney, and C. O'Dwyer, *Sci. Technol. Adv. Mater.* **17**, 563 (2016).
- ¹²C. O'Dwyer, *Adv. Mater.* **28**, 5681 (2016).
- ¹³V. Likodimos, *Appl. Catal., B* **230**, 269 (2018).
- ¹⁴S. Fraden, A. J. Hurd, and R. B. Meyer, *Phys. Rev. Lett.* **63**, 2373 (1989).
- ¹⁵M. Mittal, P. P. Lele, E. W. Kaler, and E. M. Furst, *J. Chem. Phys.* **129**, 064513 (2008).
- ¹⁶B. Bharti, F. Kogler, C. K. Hall, S. H. L. Klapp, and O. D. Velev, *Soft Matter* **12**, 7747 (2016).
- ¹⁷D. R. E. Snoswell, C. L. Bower, P. Ivanov, M. J. Cryan, J. G. Rarity, and B. Vincent, *New J. Phys.* **8**, 267 (2006).
- ¹⁸N. Elsner, C. P. Royall, B. Vincent, and D. R. E. Snoswell, *J. Chem. Phys.* **130**, 154901 (2009).
- ¹⁹N. Li, H. D. Newman, M. Valera, I. Saika-Voivod, and A. Yethiraj, *Soft Matter* **6**, 876 (2010).
- ²⁰J. Juárez and M. A. Bevan, *Adv. Funct. Mater.* **22**, 3833 (2012).
- ²¹J. J. Juárez, S. E. Feicht, and M. A. Bevan, *Soft Matter* **8**, 94 (2012).
- ²²M. E. Leunissen, H. R. Vutukuri, and A. van Blaaderen, *Adv. Mater.* **21**, 3116 (2009).
- ²³J. Crassous, A. M. Mihut, E. Wernersson, P. Pfeleiderer, J. Vermant, P. Linse, and P. Schurtenberger, *Nat. Commun.* **5**, 5516 (2014).
- ²⁴J. J. Juárez and M. A. Bevan, *J. Chem. Phys.* **131**, 134704 (2009).
- ²⁵E. V. Yakovlev, K. A. Komarov, K. I. Zaytsev, N. P. Kryuchkov, K. I. Koshelev, A. K. Zotov, D. A. Shelestov, V. L. Tolstoguzov, V. N. Kurlov, A. V. Ivlev, and S. O. Yurchenko, *Sci. Rep.* **7**, 13727 (2017).
- ²⁶P. V. Ovcharov, N. P. Kryuchkov, K. I. Zaytsev, and S. O. Yurchenko, *J. Phys. Chem. C* **121**, 26860 (2017).
- ²⁷A. Azari, J. J. Crassous, A. M. Mihut, E. Bialik, P. Schurtenberger, J. Stenhammar, and P. Linse, *Langmuir* **33**, 13834 (2017).
- ²⁸Z. M. Sherman, D. Ghosh, and J. W. Swan, *Langmuir* **34**, 7117 (2018).
- ²⁹C. Shih, J. J. Molina, and R. Yamamoto, *Soft Matter* **14**, 4520 (2018).
- ³⁰K. Müller, N. Osterman, D. Babić, C. N. Likos, J. Dobnikar, and A. Nikoubashman, *Langmuir* **30**, 5088 (2014).
- ³¹N. Osterman, I. Poberaj, J. Dobnikar, D. Frenkel, P. Ziherl, and D. Babić, *Phys. Rev. Lett.* **103**, 228301 (2009).
- ³²D. Du, D. Li, M. Thakur, and S. L. Biswal, *Soft Matter* **9**, 6867 (2013).
- ³³J. Byrom and S. L. Biswal, *Soft Matter* **9**, 9167 (2013).
- ³⁴I. Martchenko, J. J. Crassous, A. M. Mihut, E. Bialik, A. M. Hirt, C. Rufier, A. Menzel, H. Dietsch, P. Linse, and P. Schurtenberger, *Soft Matter* **12**, 8755 (2016).
- ³⁵A. T. Pham, Y. Zhuang, P. Detwiler, J. E. S. Socolar, P. Charbonneau, and B. B. Yellen, *Phys. Rev. E* **95**, 052607 (2017).
- ³⁶D. Du, F. Toffoletto, and S. L. Biswal, *Phys. Rev. E* **89**, 043306 (2014).
- ³⁷D. Du and S. L. Biswal, *Phys. Rev. E* **90**, 033310 (2014).
- ³⁸A. Weddemann, F. Wittbracht, B. Eickenberg, and A. Hütten, *Langmuir* **26**, 19225 (2010).
- ³⁹A. C. H. Coughlan and M. A. Bevan, *J. Chem. Phys.* **147**, 074903 (2017).
- ⁴⁰J. E. Martin and A. Snezhko, *Rep. Prog. Phys.* **76**, 126601 (2013).
- ⁴¹S. H. Klapp, *Curr. Opin. Colloid Interface Sci.* **21**, 76 (2016).
- ⁴²H. Löwen, *Phys. Rep.* **237**, 249 (1994).
- ⁴³B. Li, D. Zhou, and Y. Han, *Nat. Rev. Mater.* **1**, 15011 (2016).
- ⁴⁴T. Palberg, *J. Phys.: Condens. Matter* **26**, 333101 (2014).
- ⁴⁵M. N. van der Linden, D. El Masri, M. Dijkstra, and A. van Blaaderen, *Soft Matter* **9**, 11618 (2013).
- ⁴⁶A. Yethiraj, *Soft Matter* **3**, 1099 (2007).
- ⁴⁷C. Eisenmann, U. Gasser, P. Keim, G. Maret, and H. H. von Grünberg, *Phys. Rev. Lett.* **95**, 185502 (2005).
- ⁴⁸D. Du, M. Doxastakis, E. Hilou, and S. L. Biswal, *Soft Matter* **13**, 1548 (2017).
- ⁴⁹T. D. Edwards and M. A. Bevan, *Langmuir* **30**, 10793 (2014).
- ⁵⁰K. A. Komarov, N. P. Kryuchkov, and S. O. Yurchenko, *Soft Matter* **14**, 9657 (2018).
- ⁵¹J.-P. Hansen and H. Löwen, *Annu. Rev. Phys. Chem.* **51**, 209 (2000).
- ⁵²H. Löwen, *J. Phys.: Condens. Matter* **4**, 10105 (1992).
- ⁵³P. Hartmann, G. J. Kalman, Z. Donkó, and K. Kutasi, *Phys. Rev. E* **72**, 026409 (2005).
- ⁵⁴W.-K. Qi, S.-M. Qin, X.-Y. Zhao, and Y. Chen, *J. Phys.: Condens. Matter* **20**, 245102 (2008).
- ⁵⁵W.-K. Qi, Z. Wang, Y. Han, and Y. Chen, *J. Chem. Phys.* **133**, 234508 (2010).
- ⁵⁶I. L. Semenov, S. A. Khrapak, and H. M. Thomas, *Phys. Plasmas* **22**, 114504 (2015).
- ⁵⁷Z. Donkó, G. J. Kalman, and P. Hartmann, *J. Phys.: Condens. Matter* **20**, 413101 (2008).
- ⁵⁸P. Hartmann, A. Douglass, J. C. Reyes, L. S. Matthews, T. W. Hyde, A. Kovács, and Z. Donkó, *Phys. Rev. Lett.* **105**, 115004 (2010).
- ⁵⁹S. O. Yurchenko, *J. Chem. Phys.* **140**, 134502 (2014).
- ⁶⁰S. O. Yurchenko, N. P. Kryuchkov, and A. V. Ivlev, *J. Chem. Phys.* **143**, 034506 (2015).
- ⁶¹A. Yazdi, M. Heinen, A. Ivlev, H. Löwen, and M. Sperl, *Phys. Rev. E* **91**, 052301 (2015).
- ⁶²S. O. Yurchenko, N. P. Kryuchkov, and A. V. Ivlev, *J. Phys.: Condens. Matter* **28**, 235401 (2016).
- ⁶³S. Khrapak, *J. Chem. Phys.* **148**, 146101 (2018).
- ⁶⁴N. P. Kryuchkov, S. A. Khrapak, and S. O. Yurchenko, *J. Chem. Phys.* **146**, 134702 (2017).
- ⁶⁵S. Jäger, H. Schmidle, and S. H. L. Klapp, *Phys. Rev. E* **86**, 011402 (2012).
- ⁶⁶S. Jäger, H. Stark, and S. H. L. Klapp, *J. Phys.: Condens. Matter* **25**, 195104 (2013).
- ⁶⁷S. Jäger and S. H. L. Klapp, *Soft Matter* **7**, 6606 (2011).
- ⁶⁸H. Schmidle and S. H. L. Klapp, *J. Chem. Phys.* **134**, 114903 (2011).
- ⁶⁹F. Smallenburg and M. Dijkstra, *J. Chem. Phys.* **132**, 204508 (2010).
- ⁷⁰L. Bocquet, E. Trizac, and M. Aubouy, *J. Chem. Phys.* **117**, 8138 (2002).
- ⁷¹A. Ishihara, *Statistical Physics* (AP, 1971).
- ⁷²D. Frenkel and B. Smit, *Understanding Molecular Simulation: From Algorithms to Applications* (Elsevier Science, 2001).
- ⁷³J. Kolafa and M. Rottner, *Mol. Phys.* **104**, 3435 (2006).
- ⁷⁴D. Frenkel and A. J. Ladd, *J. Chem. Phys.* **81**, 3188 (1984).
- ⁷⁵A. R. Imre, G. Mayer, G. Hází, R. Rozas, and T. Kraska, *J. Chem. Phys.* **128**, 114708 (2008).
- ⁷⁶E. Luijten and H. W. J. Blöte, *Phys. Rev. Lett.* **89**, 025703 (2002).
- ⁷⁷J.-P. Hansen and I. McDonald, *Theory of Simple Liquids* (Academic, London, 1976).

⁷⁸E. P. Bernard and W. Krauth, *Phys. Rev. Lett.* **107**, 155704 (2011).

⁷⁹D. E. Dudalov, E. N. Tsiok, Y. D. Fomin, and V. N. Ryzhov, *J. Chem. Phys.* **141**, 18C522 (2014).

⁸⁰S. C. Kapfer and W. Krauth, *Phys. Rev. Lett.* **114**, 035702 (2015).

⁸¹V. N. Ryzhov, E. E. Tareyeva, Y. D. Fomin, and E. N. Tsiok, *Phys.-Usp.* **60**, 857 (2017).

⁸²L. Landau and E. Lifshitz, *Statistical Physics* (Elsevier Science, 2013), Vol. 5.